Motion Correction Via Nonrigid Coregistration of Dynamic MR Mammography Series

Andrzej Krol[1,4,2], Alphonso Magri[2], Mehmet Unlu[4], David Feiglin[1], Edward Lipson[2,1,4], James Mandel[3], Gwen Tillapaugh-Fay[1], Wei Lee[1], Ioana Coman[1,4,5] and Nikolaus M Szeverenyi[1]

[1]Department of Radiology, SUNY Upstate Medical University, Syracuse NY 13210
[2]Department of Physics, Syracuse University, Syracuse NY 13244
[3]Department of Civil and Environmental Engineering, Syracuse University, Syracuse NY 13244
[4]Department of Electrical Eng. and Comp. Science, Syracuse University, Syracuse NY 13244
[5]Department of Computer Science, Ithaca College, Ithaca, NY 14850

ABSTRACT

The objectives of this investigation are to improve quality of subtraction MR breast images and improve accuracy of time-signal intensity curves (TSIC) related to local contrast-agent concentration in dynamic MR mammography. The patients, with up to nine fiducial skin markers (FSMs) taped to each breast, were prone with both breasts suspended into a single well that housed the receiver coil. After a preliminary scan, paramagnetic contrast agent gadopentate digmeglumine (Gd) was delivered intravenously, followed by physiological saline. The field of view was centered over the breasts. We used a gradient recalled echo (GRE) technique for pre-Gd baseline, and five more measurements at 60s intervals. Centroids were determined for corresponding FSMs visible on pre-Gd and any post-Gd images. This was followed by segmentation of breast surfaces in all dynamic-series images, and meshing of all post-Gd breast images. Tetrahedral volume and triangular surface elements were used to construct a finite element method (FEM) model. We used ANSYS™ software and an analogy between orthogonal components of the displacement field and the temperature differences in steady-state heat transfer (SSHT) in solids. The floating images were warped to a fixed image using an appropriate shape function for interpolation from mesh nodes to voxels. To reduce any residual misregistration, we performed surface matching between the previously warped floating image and the target image. Our method of motion correction via nonrigid coregistration yielded excellent differential-image series that clearly revealed lesions not visible in unregistered differential-image series. Further, it produced clinically useful maximum intensity projection (MIP) 3D images.

Keywords: Nonrigid registration, deformable models, motion correction, dynamic breast MRI, differential images, time-signal intensity curves.

1. INTRODUCTION

Breast cancer is one of the most common cancers among women in the U.S.[1,2]. Early detection and treatment is very important in the successful treatment and outcome of breast cancer care. It has been demonstrated that MR scan pulse sequences and protocols optimized for breast cancer imaging, including high-resolution 3D sequences with MR dynamic imaging using a Gd contrast agent [3,4,5], result in improved diagnostic accuracy along with confidence of radiologists interpreting examinations. These MR breast scan examinations also result in faster diagnosis and are a useful adjunct to conventional x-ray mammography and ultrasonography from ambiguous cases. In this study, we investigated image data analysis methods that can be applied to improve quality of dynamic MR breast scan results and improve accuracy of the obtained time-signal intensity curves (TSIC) related to the local contrast agent concentration in dynamic MR mammography (MRM).

2. MATERIALS AND METHODS

MR mammography was performed on a Philips Intera 1.5 T MRI system with a standard Philips clinical breast RF receiver coil. The patient was prone with both breasts suspended in a single well housing the receiver coil. Prior to scanning, up to nine fiducial skin markers (FSMs) were taped to each breast. An IV line was established in a distal antecubital vein with a 22 or 24 gauge angiocatheter insertion for Gd-DTPA (Magnevist; Berlex Imaging) injection. After scan acquisition of the pre-Gd scan the contrast (0.15 mmol/kg) was delivered with a constant flow of 10 ml/15s and followed directly by 20 ml of physiologic saline solution. The field of view (360 mm $\times$ 360 mm) was centered over the breasts. We used a gradient recalled echo (GRE) technique with TR/TE = 5.4/2.1 for pre-Gd baseline reference, followed by five more measurements at 60s intervals (in a 256 $\times$ 256 matrix). We implemented an iterative approach to nonrigid image registration[6,7]. In this process the target image is the pre-Gd image and the floating images are the n^{th} post-Gd images. In the first phase, corresponding FSMs visible on pre-Gd and any post-Gd images are identified, and their geometrical centroids are found using a knowledge-based semi-automated algorithm allowing estimation of FSM displacement vectors. This is followed by segmentation of breast surfaces in all dynamic series images and meshing of all the post-Gd breast images. In this procedure, the tetrahedral volume elements and triangular surface elements are used to construct a finite element method (FEM) model. A dense displacement field is estimated by first distributing the Cartesian components of the observed FSM displacement vectors linearly over the breast surface, and then distributing them throughout the breast volume (Fig. 1). Since this linear displacement distribution can be described by the Laplace-Poisson equation, an analogy between orthogonal components of the displacement field and the temperature field in steady-state heat transfer (SSHT) in solids is used via standard heat-conduction FEM software with conductivity of surface elements set significantly higher (here by a factor of 1,000) than that of volume elements. A commercial FEM package (ANSYS) is used for meshing and FEM calculations. Finally, the floating image is warped to a fixed image using an appropriate shape function for interpolation from mesh nodes to voxels. However, we have found that such processing might still result in some misregistration in the regions away from FSMs. Therefore, in the second phase, we perform surface matching between the previously warped floating image and the target image. This is done by estimating differences between nearest points on the multiple sagittal cross-sections through the two breast volumes of interest and using such differences as loads (displacements vectors) in our FEM. As a result, all the residual misregistration of the two volumes is significantly reduced.

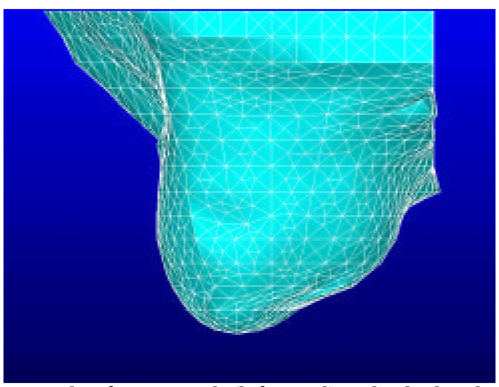

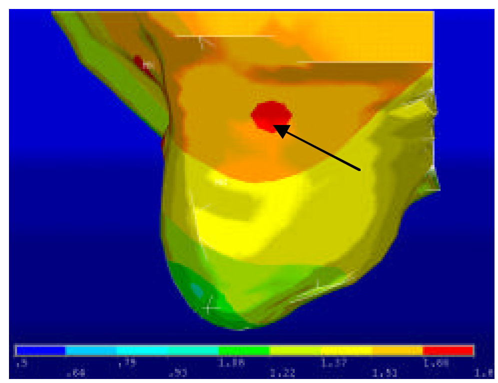

Fig. 1. Example of FEM mesh (left panel) and calculated marker displacement distribution in x direction (right panel) used in the first iteration of FEM model for a floating breast MR image. Arrow indicates location of a fiducial marker. Displacements are in millimeter units.

4. RESULTS

After the registration steps have been applied, two types of dynamic images were created: i) baseline-subtracted (pre-Gd image subtracted from the N^{th} time frame) and ii) differential (the $[N-1]^{th}$ time frame image subtracted from the N^{th} time frame image) The obtained baseline–subtracted differential images are shown in axial views (Figs. 2 and 3). Twelve regions of interest (ROIs) labeled with numbers that are used to plot mean pixel intensity vs. time are defined in the baseline-subtracted image in axial views (Fig. 2) and in differential images in axial view (Fig. 3). The baseline-subtracted time-signal intensity curves (TSICs) are shown in Fig. 4a and the differential TSICs are shown in Fig. 4b,c,d The twelve ROI's where chosen to investigate TSIC changes in ROIs located in breast tissue areas that show an increase (wash-in), decrease (wash-out), or no response (normal) to Gd-DTPA contrast vs. time after injection in unregistered images, as compared to registered images. Average pixel intensity value error for baseline-subtracted images is an intensity value of seven and for differential images is an intensity value of four. TSIC characteristics in each ROI were investigated. Five measurements were taken and recorded: a) the maximum pixel intensity and the b) minimum pixel intensity in a ROI through all time frames; c) *R* value for the best fit (of a second order polynomial for a TSIC), d) integrated intensity (found by calculating the area under each fitted TSIC) and e) initial slope of the best fit. The obtained values are collected in Tables 1 and 2 for the baseline-subtracted and for the differential images, respectively.

5. CONCLUSIONS

Application of our FEM deformable model to the nonrigid coregistration of dynamic MRI breast images has yielded improved baseline-subtracted images (Fig. 2). They allow better definition of the tissue regions with increased uptake and washout, as compared to the unregistered images. The coregistered dynamic images demonstrate structures that otherwise are difficult to detect or cannot be seen in the unregistered dynamic images. This is confirmed by the plots of the time-signal intensity curves (Fig. 4). We observe that the area under TSICs and the absolute value of the slope of the fitted TSICs in wash-in and wash-out regions increases after coregistration (Table 1). The TSICs in the "normal" regions do not change their characteristics after nonrigid coregistration. We observe image-quality improvement in the coregistered differential images (Fig. 3). However, the TSICs in the selected ROIs are practically unchanged by the registration process (Fig.4). The proposed FEM method for motion correction in dynamic MRM series is very promising and could improve diagnostic performance of MRM. However, clinical implementation of this method would require creation of a semi-automated-processing software pipeline that would minimize human intervention and processing time.

6. ACKNOWLEDGMENTS

This research was sponsored in part by a Carol M. Baldwin Breast Cancer Research Award.

7. REFERENCES

1. Boring, C.C., Squires, T.S., Tong, T., Montgomery, S., "Cancer statistics, 1994", CA: a Cancer Journal for Clinicians, 44(1), 7-26, 1994.

2. American Cancer Society, What Are the Key Statistics for Breast Cancer?, http://www.cancer.org, 2004.

3. Gibbs, P., Liney, G. P., Lowry, M., Kneeshaw, P. J., Turnbull, L. W., "Differentiation of benign and malignant sub-1 cm breast lesions using dynamic contrast enhanced MRI", Breast, 13(2), 115-21, 2004.

4. Eliat, P. A., Dedieu, V., Bertino, C., Boute, V., Lacroix, J., Constans, J. M., de Korvin, B., Vincent, C., Bailly, C., Joffre, F., de Certaines, J., Vincensini, D., "Magnetic resonance imaging contrast-enhanced relaxometry of breast tumors: an MRI multicenter investigation concerning 100 patients", Magnetic Resonance Imaging, 44(4), 475-81, 2004.

5. Vomweg, T. W., Teifke, A., Kunz, R. P., Hintze, C., Hlawatsch, A., Kern, A., Kreitner, K. F., Thelen, M., "Combination of low and high resolution sequences in two orientations for dynamic contrast-enhanced MRI of the breast: more than a compromise", European Radiology, 14(10), 1732-42, 2004.

6. Krol, A. , Unlu, M. Z., Baum, K. G., Mandel, J. A., Lee, W., Coman, I. L., Lipson, E. D., Feiglin, D. H., "MRI/PET nonrigid breast-image registration using skin fiducial markers" *Physica Medica*, 2005

7. Unlu, M. Z., Krol, A., Coman, I. L., Mandel, J. A., Baum, K. G., Lee, W., Lipson, E. D., Feiglin, D. H., "Deformable Model for 3D Intramodal Nonrigid Breast Image Registration with Fiducial Skin Markers", *Proceedings of SPIE*, 5747, 1528-1534, 2005.

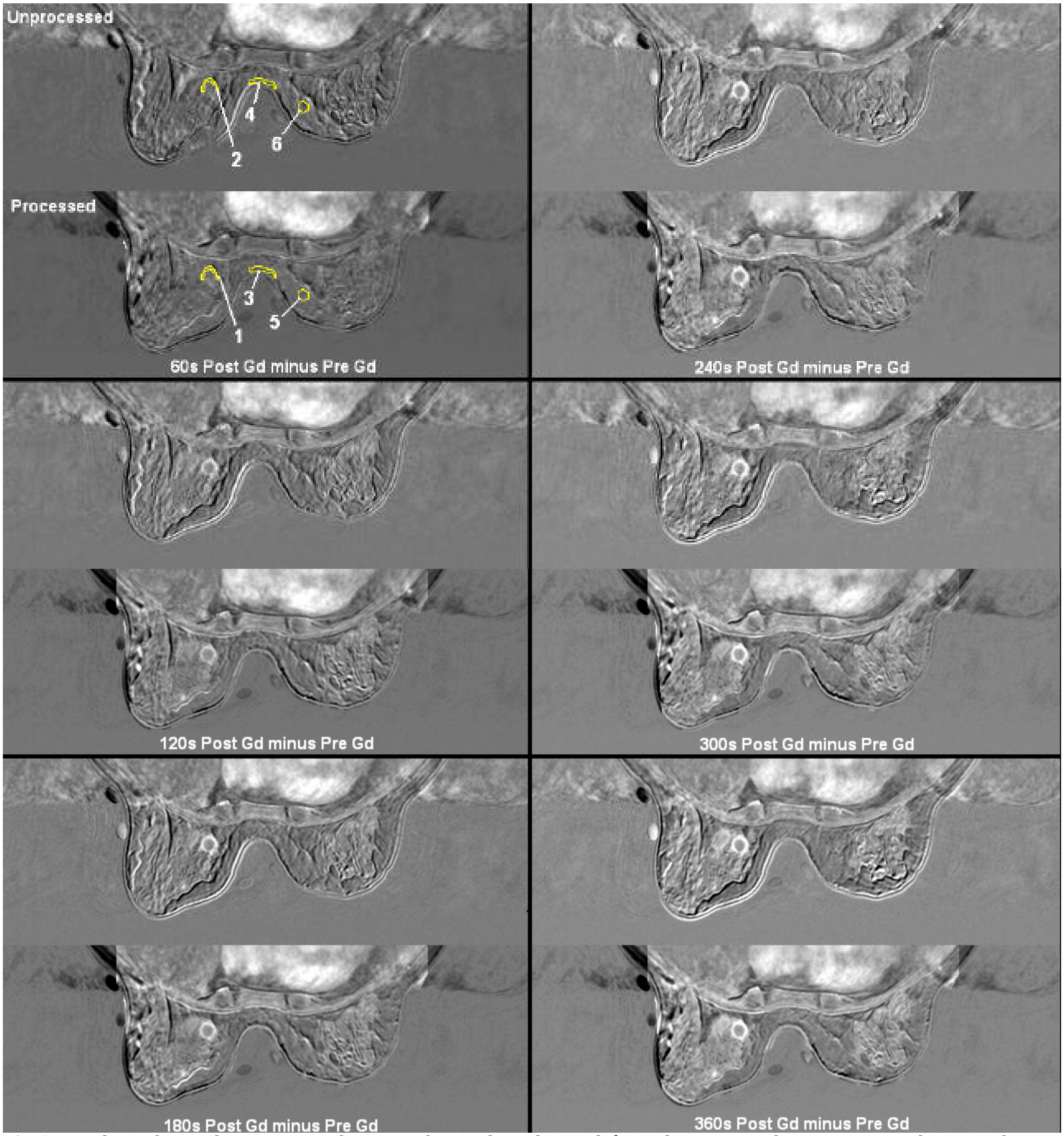

Fig. 2. Baseline-subtracted images in axial views with, as indicated in top left panel, unprocessed images at top and processed images at bottom of each panel depicting a single time frame. The top left panel shows regions of interest that were used to obtain plots of mean pixel intensity vs. time (Fig. 4).

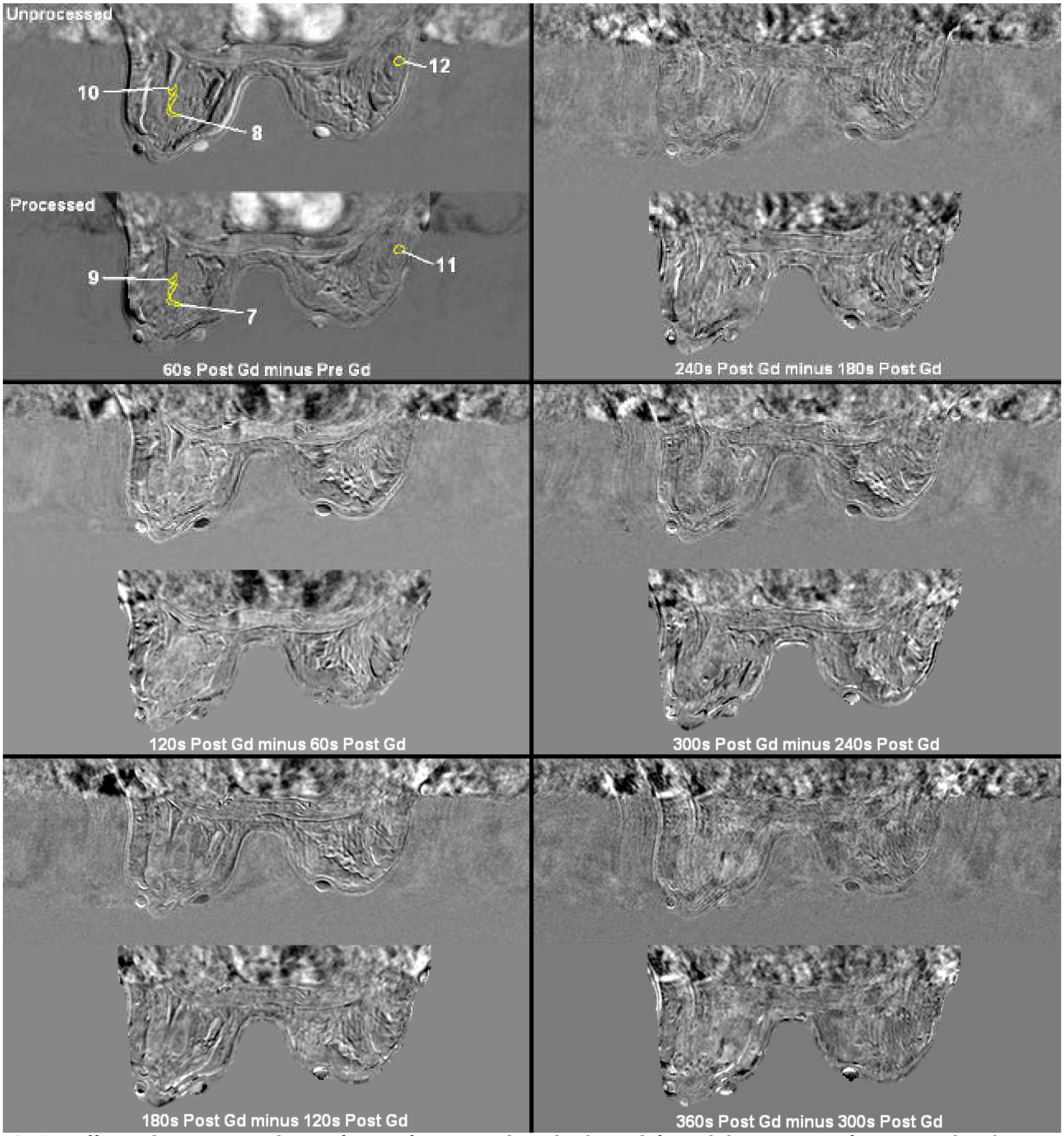

Fig. 3. Differential images in axial views for time frames as indicated. The top left panel shows regions of interest used to obtain plots of mean pixel intensity vs. time (Fig. 4).

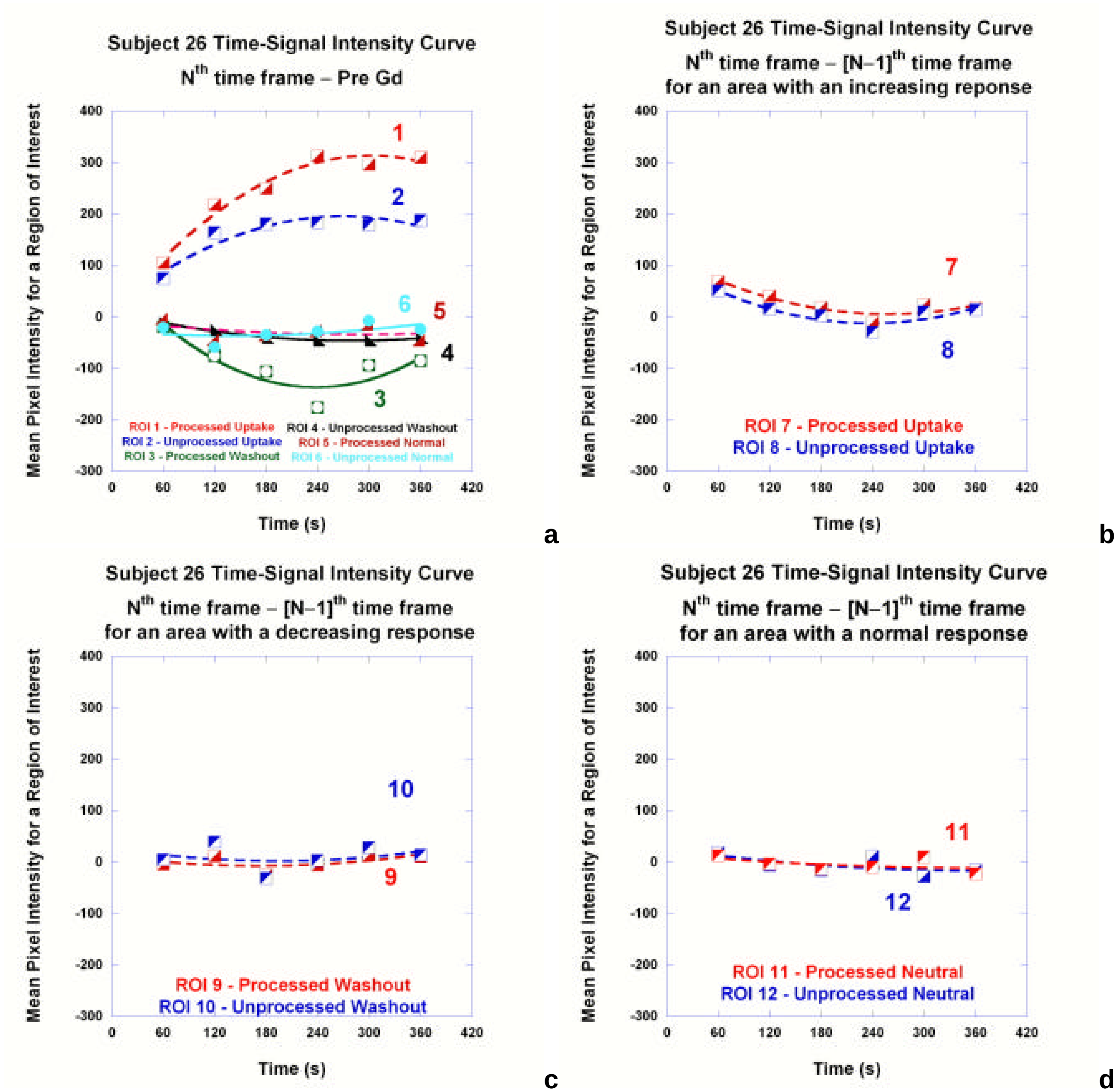

Fig. 4. In all cases the second-order polynomial TSIC curves were fitted to the data. **a.** ROIs defined in Fig. 2 from baseline-subtracted images in axial view. **b.c.d.** ROIs defined in Fig3. from differential images in axial view

Table 1. Parameters obtained for ROI's defined in Fig. 2. Second-order polynomial TSIC curves were fit to the data. Initial slope denotes that of the fitted curve at the first data point. The integrated intensity was estimated using the fitted curve.

Parameters of baseline-subtracted TSICs in axial views	ROI 1 Processed uptake ROI	ROI 2 Unprocessed uptake ROI	ROI 3 Processed washout ROI	ROI 4 Unprocessed washout ROI	ROI 5 Processed normal ROI	ROI 6 Unprocessed normal ROI
Maximum pixel intensity	465	498	76	253	42	84
Minimum pixel intensity	10	-52	-384	-254	-133	-215
Integrated intensity	1494	970	-557	-210	-171	-175
Initial slope	1.65	1.02	-1.38	-0.32	-0.15	-0.07
R value	0.98	0.94	0.89	0.996	0.39	0.52

Table 2. Parameters obtained for ROI's defined if Fig. 3. Second-order polynomial TSIC curves were fit to the data. Initial slope denotes the slope of the fitted curve at the first data point. The integrated intensity was estimated using the fitted curve.

Parameters of differential TSICs in axial views	ROI 7 Processed uptake ROI	ROI 8 Unprocessed uptake ROI	ROI 9 Processed washout ROI	ROI 10 Unprocessed washout ROI	ROI 11 Processed normal ROI	ROI 12 Unprocessed normal ROI
Maximum pixel intensity	181	222	80	119	204	168
Minimum pixel intensity	-123	-95	-82	-75	-75	-91
Integrated intensity	162	63	1	57	-27	-35
Initial slope	-0.66	-0.72	-0.14	-0.18	-0.12	-0.20
R value	0.92	0.91	0.56	0.29	0.53	0.66